PROFESSOR PAULINE E JULLIEN (Orcid ID : 0000-0003-1212-3246)

Article type : Original Article

Functional characterization of *Arabidopsis* ARGONAUTE 3 in reproductive tissues

Pauline E. Jullien[1,2], Stefan Grob[3], Antonin Marchais[1], Nathan Pumplin[1], Clement Chevalier[1], Diane M.V. Bonnet[2], Caroline Otto[1], Gregory Schott[1] and Olivier Voinnet[1]

[1] Institute of Molecular Plant Biology, Swiss Federal Institute of Technology Zurich (ETH-Zurich), Zurich, Switzerland.

[2] Institute of Plant Sciences, University of Bern, Bern, Switzerland.

[3] Department of Plant and Microbial Biology, University of Zurich and Zurich-Basel Plant Science Center, University of Zurich, Zurich, Switzerland.

Author ORIC IDs:

Pauline E. Jullien (#0000-0003-1212-3246), Stefan Grob (#0000-0001-6199-7383), Antonin Marchais (#0000-0003-0954-8294)

For correspondence:

Pauline E. Jullien (pauline.jullien@ips.unibe.ch)

short running title

Characterization of Arabidopsis ARGONAUTE 3

Keywords
Seeds, *Arabidopsis*, small RNA, Argonautes, AGO3, reproduction

SUMMARY
Arabidopsis encodes ten ARGONAUTE (AGO) effectors of RNA silencing, canonically loaded with either 21-22 nucleotide (nt) long small RNAs (sRNA) to mediate post-transcriptional-gene-silencing (PTGS) or 24nt sRNAs to promote RNA-directed-DNA-methylation. Using full-locus constructs, we characterized the expression, biochemical properties, and possible modes of action of AGO3. Although *AGO3* arose from a recent duplication at the *AGO2* locus, their expression patterns differ drastically, with AGO2 being expressed in both male and female gametes whereas AGO3 accumulates in aerial vascular terminations and specifically in chalazal seed integuments. Accordingly, *AGO3* down-regulation alters gene expression in siliques. Similar to AGO2, AGO3 binds sRNAs with a strong 5'-adenosine bias, but unlike *Arabidopsis* AGO2, it binds most efficiently 24nt sRNAs. AGO3 immunoprecipitation experiments in siliques revealed that these sRNAs mostly correspond to genes and intergenic regions in a manner reflecting their respective accumulation from their loci-of-origin. AGO3 localizes to the cytoplasm and co-fractionates with polysomes to possibly mediate PTGS via translation inhibition.

INTRODUCTION

RNA silencing is an ancient mechanism found in plants, animals, and fungi that controls endogenous gene expression and fends off invasive nucleic acids including viruses and transposable elements. RNA silencing relies on the production of small RNAs (sRNAs) (Bologna and Voinnet, 2014) by DICER-LIKE RNase-III enzymes (DCL) cleaving double-stranded RNA (dsRNA) precursors. sRNAs are loaded into effector proteins called Argonautes (AGOs), which mediate sequence-specific post-transcriptional gene silencing (PTGS) at the mRNA level, or transcriptional gene silencing (TGS) at the chromatin level. The loading specificity for AGO proteins relies, at least partly, on the length and identity of the 5' terminal nucleotide of the sRNAs (Mi *et al.*, 2008).

The *Arabidopsis* genome encodes ten *AGOs*, which are phylogenetically divided into three distinct clades, namely *AGO4-6-8-9*, *AGO1-5-10,* and *AGO2-3-7*, indicating potential functional redundancy within these clades (Mallory and Vaucheret, 2010). The *AGO4-6-8-9* clade is involved in TGS by RNA-directed-DNA-Methylation (RdDM) and its members are collectively referred to as the "RdDM AGOs". AGO4, the most ubiquitous and best-studied member of this clade, recruits the DNA methyltransferase DRM2 to target loci to catalyse cytosine methylation (Zilberman *et al.*, 2003; Law and Jacobsen, 2010; Zhong *et al.*, 2014). AGO6 acts in partial redundancy with AGO4 but is less ubiquitously expressed and is able to target RdDM via loading of 24nt sRNAs (Zheng *et al.*, 2007; Havecker *et al.*, 2010). AGO9 has a specific role during reproduction (Olmedo-Monfil *et al.*, 2010) whereas *AGO8* is expressed but its open reading frame displays a premature stop codon (Takeda *et al.*, 2008). The *AGO1-5-10* clade is involved in PTGS and is mainly linked to micro RNAs (miRNAs) (Zhu *et al.*, 2011; Bologna and Voinnet, 2014). AGO1, the main member of this clade loads predominantly miRNAs in healthy plants and is ubiquitously expressed (Bologna and Voinnet, 2014). As a consequence, *ago1* mutants display strong pleiotropic phenotypes. AGO10 regulates shoot apical meristem development by binding miR165/166 (Zhu *et al.*, 2011; Liu *et al.*, 2009). Wild-type functions for AGO5, which displays a 5'C bias and binds 21nt, 22nt and 24nt siRNAs (Mi *et al.*, 2008), remain unclear, but an *ago5* dominant mutant allele prevents female gametophyte development (Tucker *et al.*, 2012).

The last clade, comprising *AGO2-3-7* seems to have more specialized functions. AGO7 is involved in the trans-acting (ta)siRNA pathway: loaded with miR390, it targets non-coding TAS3 transcripts for

cleavage, resulting in production of secondary siRNAs that regulate the expression of AUXIN RESPONSE FACTORs (ARF3 and ARF4), which are important for the establishment of leaf polarity (Fahlgren *et al.*, 2006; Montgomery *et al.*, 2008). Like AGO1, *Arabidopsis* AGO2 serves a role in antiviral silencing against *Turnip crinkle virus* (TCV) and other viruses (Harvey *et al.*, 2011; Jaubert *et al.*, 2011; Carbonell *et al.*, 2012; Pumplin and Voinnet, 2013). AGO2 is also involved in resistance against the phytopathogenic bacterium *Pseudomonas syringae* by binding the miR393 passenger strand (miR393*) to regulate PR1 protein secretion (Zhang *et al.*, 2011). AGO2 has been shown to regulate Plantacyanin by binding miR408 (Maunoury and Vaucheret, 2011). Finally, AGO2 has been also implicated in double-stand break repair upon genotoxic treatments (Wei *et al.*, 2012). Interestingly, in contrast to the PTGS involvement of other member of its clade, AGO3 has been described to preferentially bind 5'adenosine 24nt transposon-related sRNAs upon salt stress (Zhang *et al.*, 2016). AGO3 mis-expression could partially complement an *ago4* mutation, suggesting a role in TGS rather than PTGS pathway.

Beside data available under salt-stress conditions, the expression pattern, sRNA loading capacity, potential roles and mode(s) of action of AGO3 during *Arabidopsis* development have eluded investigation so far. In this study, we conducted a functional characterization of *Arabidopsis* AGO3, which, together with its closest homolog AGO2, represent a unique clade among the plant AGOs containing the PIWI-domain catalytic triad DDD motif. *AGO3* arose from a recent duplication event at the *AGO2* locus, resulting in highly similar proteins but unrelated promoter sequences that cause distinct and specific expression patterns, including in reproductive tissues, the main focus of our study.

RESULTS AND DISCUSSION

AGO2 and *AGO3* arose from a recent duplication

AGO2 and *AGO3* are organized directly in tandem on *Arabidopsis* chromosome 1. To investigate the locus structure in detail, we generated a dot-plot representation of the locus' self-alignment (Figure 1a). This led to the identification of a duplication break-point in the first exon within an *AtCOPIA* transposon-containing region (*AtCopia27-AT1TE36140* in *AGO2* and *AtCopia28-AT1TE36160* in

AGO3;(Buisine *et al.*, 2008)). The corresponding region encodes for numerous glycines and arginines (34%G and 12%R in *AGO3* first exon) and thus, referred to as "glycine-rich-repeat" or GRR. The GRR region itself is duplicated in *AGO3* compared to *AGO2*, giving rise to a significantly longer exon 1 (949bp in *AGO3* as opposed to 421bp in *AGO2*). The remaining exon 2 and 3, coding for the conserved PAZ and PIWI domains, display 74.16% amino acid identity between AGO3 and AGO2 as opposed to only 38.12% with AGO1 and 29.6% with AGO4.

To trace the origin of the *AGO2/AGO3* duplication, we analyzed the syntenic organization of the AGO2/AGO3 locus in related plant species using the CoGe platform (Lyons and Freeling, 2008). The AGO2/AGO3 duplication is conserved between *Arabidopsis thaliana* and *Capsella rubella,* but not with *Cardamine hirsuta,* showing that this duplication event occurred recently within the Lineage I of the Brassicaceae according to the recent phylogeny from Nikolov *et al.* (Figure 1b) (Nikolov *et al.*, 2019). The tandem duplication is absent from more distant Brassicaceae of Lineage IV such as *Arabis Alpina* and of Lineage II such as *Eutrema salsugineum* (Figure S1).

Further phylogenic analyses using putative AGOs from various plant species (Figures 1c, Figure S2a-b and Table S5) revealed that DDD AGO likely arose in seed plants. The amino acids of the PIWI-domain catalytic triad (DDD) required for RNA endonucleolytic cleavage are conserved between AGO2 and AGO3 but differ from the DDH triad found in all other *Arabidopsis* AGOs (Figure S3a). The presence of this catalytic triad and the previous findings that AGO2 is slicing-proficient, suggest that AGO3 also has endonucleolytic cleavage capacities (Poulsen *et al.*, 2013; Carbonell *et al.*, 2012). Close inspection of the sequence alignments of AGOs from the AGO2/AGO3 clade (Figure S3b) revealed that the DDD motif is conserved within this clade. Several Angiosperms contain two or more AGOs with the DDD triad (Figure 1c, S2a, S3b). Hence, the duplication of DDD-containing AGOs seems to have occurred several independent times in evolution.

AGO2 and AGO3 show cell-specific expression during reproduction

The *AGO2* and *AGO3* promoters were not affected by the duplication event (Figure 1a), suggesting that AGO2 and AGO3 might have distinct expression patterns. To address this question in detail, we stably expressed full-locus fluorescent protein fusions under their native promoters (the promoter sequences used are depicted in Figure 1a), referred to as p*AGO3*:*mCherry-AGO3* and

p*AGO2:mCherry-AGO2*. In light of online public expression profiles, we primarily focused our analyses on reproductive tissues (Winter *et al.*, 2007). The expression of the reporter constructs was imaged in plants co-expressing *LIG1-GFP* as a ubiquitous nuclear marker, in order to facilitate tissue recognition within the developing seeds.

p*AGO3*:*mCherry-AGO3* expression was detected in a few cells in the chalazal integument of ovules and seeds (Figure 2a-b), consistent with previously published laser-capture (LCM)-based expression data (Belmonte *et al.*, 2013). The fluorescent signal of p*AGO3:mCherry-AGO3* increases during early stages of seed development (Figure 2a-b). We could not detect the mCherry-AGO3 signal within the female gametophyte, the male gametophyte, or in the embryo and endosperm, which develop after fertilization. p*AGO3:mCherry-AGO3* expression was also detected in regions proximal to vasculature termination sites both at the end of stamen filaments (Figure 2c) and at the base of floral meristems (Figure 2d). In sharp contrast, p*AGO2:mCherry-AGO2* expression in analyzed reproductive organs was germline-specific, with fluorescent signals detected in egg cells of the female gametophyte (Figure 2e) and in sperm cells of the pollen grain before fertilization (Figure 2f). Note that the foci observed in sperm cells may result from previously documented aggregation artifacts caused by mCherry or cytoplasmic concentration rather than *bona fide* cytoplasmic structures or specialized compartments (Katayama *et al.*, 2008; Kremers *et al.*, 2011). Following fertilization, the p*AGO2:mCherry-AGO2* signal was neither detected in the developing endosperm nor in the developing embryo.

The *AGO2* mRNA is a known target of miR403 (Allen *et al.*, 2005). The *AGO3* transcript also contains a putative miR403 binding site located in the 3'UTR (Figure S4a-b). To test if and how miR403 influences *AGO2* and *AGO3* expression patterns, we engineered plants expressing transcriptional reporters for *AGO2* and *AGO3*, respectively named p*AGO2:H2B-mCherry* and p*AGO3:H2B-mCherry*. Both transcriptional reporters contain promoter sequences up to the translation start site, thus including the 5'UTR, but excluding the 3'UTR and thus devoid of the miR403 target site. Both reporters showed similar expression patterns in reproductive tissues compared to the respective full genomic fluorescent construct (Figure 3a-b). This result therefore excludes a strong miR403 contribution to the global tissue-specific accumulation of AGO2 and AGO3, at least under laboratory conditions. miR403 most likely regulates *AGO2* and *AGO3*

expression levels within their cognate tissues of expression. Consistent with this interpretation, both *AGO2* and *AGO3* transcripts are up-regulated in miRNA-deficient mutants of *Arabidopsis* including *ago1-27*, *hen1-6, hyl1-2* and *dcl1-11* (Figure 3c-d and S5a-b). Furthermore, since the expression patterns between transcriptional and translational fusions are similar and since neither AGO2 nor AGO3 is detected outside its cognate expression domain, both proteins are unlikely to move between cells, at least in the tissues inspected. Added to similar observations made with AGO1 in roots (Brosnan *et al.*, 2019), these results support the notion that plant AGO proteins exert their functions cell-autonomously.

We conclude that AGO2 and AGO3 display non-overlapping expression patterns in reproductive tissues. AGO3 is expressed during early stages of seed development, in a specific subset of sporophytic cells located in the proximity of aerial vasculature terminations. AGO2, by contrast, is mostly expressed in male and female gametes. Unlike that of AGO2, whose basal accumulation is also detectable in vegetative tissues, AGO3 expression is at, or below, detection levels in leaves. AGO3's confinement to vascular terminations in the apical growing tissues could suggest a spatially restricted role in antiviral defense since the phloem is employed by most plant viruses for systemic infection and unloading into sink, *i.e.* growing tissues. Testing this hypothesis will require further investigations. Despite their high amino-acid sequence identity, the expression patterns of each protein differ drastically. As such, AGO3 and AGO2 thus provide a possible example of genetic sub-functionalization.

AGO3 binds 5' adenosine sRNA primarily of 24nt in length

Sequencing of sRNAs from immunoprecipitates (IPs) has shown that AGO2 preferentially binds 21nt sRNAs with a 5'adenosine (Mi *et al.*, 2008). Upon salt stress, AGO3 was shown to bind 24nt sRNAs with a 5'adenosine bias (Zhang *et al.*, 2016). To investigate if AGO3 sRNA loading in developing siliques is comparable to its loading upon salt stress, we generated stable *Arabidopsis* lines harboring p*AGO3:FHA-AGO3*, which expresses an N-terminal Flag-epitope-tagged version of AGO3 under its cognate promoter. Western-blot analysis confirmed that those lines indeed accumulate full-length tagged AGO3 (FHA-AGO3) in silique samples (Figure S6a). The FHA-AGO3 expression pattern was consistent with the microscopy analysis in these tissues. Noteworthy, overexpression of FHA-AGO3

under the CaMV p35S promoter did not promote FHA-AGO3 over-accumulation but, instead, triggered accumulation of an AGO3-derived cleavage fragment (Figure S6a). To evaluate if FHA-AGO3 could bind sRNAs *in planta* and to assess AGO3's binding affinity, we first transiently expressed, in *N. benthamiana* leaves, FHA-AGO3 together with a *p35S-GFP* construct as an inducer of PTGS and GFP-derived sRNA as described (Iki *et al.*, 2017). Both 21nt and 24nt GFP sRNAs were detected in AGO3 immunoprecipitates (IPs) in contrast with only 21nt GFP sRNAs detected in AGO2 IPs conducted in parallel. Control IPs from AGO1 and AGO4 confirmed, as expected, selective binding of 21nt and 24nt GFP sRNAs, respectively. Therefore, unlike transiently expressed AGO2, transiently expressed AGO3 binds both 21nt and 24nt exogenous sRNAs.

In order to analyze AGO3's affinity and specificity for endogenous sRNAs, the p*AGO3:FHA-AGO3* construct was transformed into *ago3-3* mutant *Arabidopsis*. sRNAs were isolated from Flag IPs (referred to as AGO3 IPs) obtained from 1-5 days-after-pollination (DAP) siliques of p*AGO3:FHA-AGO3* plants. sRNAs isolated from Flag IPs from non-transgenic (Col-0) 1-5DAP siliques (referred to as Ctrl-IP) and total RNA from (Col-0) 1-5 DAP siliques (referred to as Total) were used as controls for Illumina-based sequencing (Figure 4 and S6b). Because AGO3 expression is restricted to chalazal integuments in siliques, we anticipated a low signal-to-noise ratio due to inherent dilution effects and low recovery of the protein. sRNA reads were aligned onto the *Arabidopsis* genome and specific enrichment was calculated along 500 bp genomic windows; sRNAs over-represented (>10-fold enrichment) in the AGO3 IP compared to Total were subsequently deemed as "AGO3-IP enriched". As a control, we similarly calculated a "Ctrl-IP -IP enriched" comparing Ctrl-IP *versus* Total. We found that, similarly to observations made on AGO2 and AGO3 IPs isolated under salt-stress conditions (Mi *et al.*, 2008; Zhang *et al.*, 2016), AGO3 exhibits a 5'adenosine (5'A) loading bias in unstressed siliques. This property was indeed shared by 90% of sRNAs in the AGO3-IP enriched population (Figure 4b; Figure S7). Unlike AGO2 (Mi *et al.*, 2008) and AGO3 in transient expression experiments (Figure 4a), AGO3 expressed in siliques of p*AGO3:FHA-AGO3* plants binds mostly 24nt sRNAs and only to a lesser extent, 21nt sRNAs (Figure 4c; Figure S7). Analyzing the genome-wide distribution of AGO3-enriched sRNAs (Figure 4d) did not reveal a significant enrichment over specific genomic regions but, rather, a uniform distribution along the five *Arabidopsis* chromosomes. This contrasts with the previously reported enrichment of AGO3-bound sRNAs along TE-rich and

intergenic regions in seedlings under salt-stress conditions. In siliques of unstressed p*AGO3:FHA-AGO3* plants, the AGO3-bound fraction was significantly enriched in sRNAs mapping to protein-coding genes as well as intergenic regions (Figure 4e). Many sRNA types bound by AGO2, including tasiRNAs, miRNAs, and miRNA*s (Mi *et al.*, 2008) are not overrepresented in the AGO3 IP-enriched fraction. Given their highly specific and non-overlapping expression patterns, the difference in sRNAs identity loaded into AGO2 and AGO3 may reflect distinct sRNA compositions in the cognate expression domains of each protein as well as different loading properties.

Northern analysis of sRNAs extracted from Flag-AGO3 IPs from 4-6 DAP siliques confirmed this distribution as well as the relative 21nt/24nt abundance of AGO3-bound sRNAs for several tested loci (Figure 4f; Figure S8a). Only 21nt sRNAs were detected at these loci in a control AGO2 IP, indicating that AGO3 binds mainly 24nt but also 21nt sRNAs in a ratio reflecting the accumulation of these sRNA species at their locus-of-origin. Furthermore, the AGO3-bound 21nt and 24nt sRNA populations were overlapping, rather than separately distributed, in specific regions of the respective loci, suggesting their processing from a common double stranded RNA (dsRNA) precursor (Figure S8a). Alternatively, some loci displayed size-specific enrichment under the form of discrete peaks (Fig S8b). Together, these results indicate that AGO3 mostly binds 24nt sRNAs in siliques; these arise from protein-coding genes as well as intergenic regions and exhibit a strong 5'A bias.

AGO3 regulates gene expression in siliques

Two *ago3* mutant alleles have been described: *ago3-1*, with a T-DNA insertion in the last exon and the misexpression-allele *ago3-2* (Takeda *et al.*, 2008). We characterized a new mutant allele (GABI_743B03), named *ago3-3,* in which the *AGO3* transcript levels were at or below qPCR detection limit in all tissues inspected (cLv, inflo, 1-4 DAP and 5-8 DAP; Figure. 5a). To investigate AGO3 expression at the protein level, we raised a polyclonal antibody against immunogenic epitopes of the native protein. The AGO3 full-length protein has a predicted molecular mass of ~130kDa. Western blot analysis revealed a band at the expected size in wild-type plants, which was absent in all *ago3-3* mutant tissues analyzed, confirming the antibody's specificity and the knockout status of the *ago3-3* allele (Figure 5b). Moreover, the relative levels of AGO3 protein accumulation in wild-type plants were in agreement with the results of the qPCR and microscopy analyses, confirming that

AGO3 expression is initially low in inflorescences and progressively up-regulated during early seed development within the siliques (Figure 5b). Noteworthy, the pattern of AGO3 accumulation remained globally unchanged in the *ago2-1* null background (Figure 5b) as were the protein levels of AGO2 in various tissues of the *ago3-3* mutant (Figure S9). Thus, AGO3 and AGO2 proteins are not subjected to cross-regulation or compensatory expression mechanisms.

To gain insight into the gene regulatory potential of AGO3-bound sRNAs, we investigated the transcriptome of *Arabidopsis* 1-5 DAP siliques in either wild-type (Col-0) or *ago3-3* mutant plants. RNA-seq libraries of two biological replicates from each genotype were subjected to Illumina-based sequencing. We found a higher number of up-regulated compared to down-regulated genes in *ago3-3* versus Col-0 siliques (63 versus 24; Figure 5c), as anticipated from AGO3 being involved in negative gene regulation via RNA silencing. Further investigation of the loci showing at least a 2-fold expression change (FDR < 0.05; Figure 5d) showed that *AGO3*-regulated genes have an unbiased distribution along the five chromosomes' arms. A GO-term analysis using agriGO (Du *et al.*, 2010) revealed a significant enrichment in "response to stimulus" among other biological processes (Table S1).

Taking into account the AGO3 expression pattern as revealed by microscopy, we refined our differential gene expression analysis during seed development by specifically focusing on the chalazal seed coat of wild-type plants, using data from Belmonte *et al* (Belmonte *et al.*, 2013). We observed that expression of genes up-regulated in *ago3-3* tends to increase during seed development, particularly at later stages (Figure 5e). In contrast, the expression of down-regulated genes in *ago3-3* remains nearly constant over the same time-window (Figure 5f). Moreover, the increased gene expression during seed development is anti-correlated with *AGO3* expression in the chalazal seed coat (Figure 5f), which decreases at later development stages. No such clear tendency was observed in the other seed compartments inspected, supporting a narrow spatio-temporal window of AGO3 action in seed development. This possibly explains the absence of seed abortion or other seed developmental phenotype in *ago3-3* mutant siliques (Figure 5g and S10).

In an attempt to identify direct targets of AGO3, we investigated potential correlations between AGO3-bound sRNAs in siliques and the differentially expressed genes (DEG) found in the *ago3-3* mutant analysis (Figure S11). The analysis was performed with DEG's coding regions to assay for

potential targets of PTGS and with DEG's promoters (1kb upstream of ATGs) to assay for potential targets of TGS. The only overlapping locus was *AGO3* itself, a likely transgenesis artefact from the pAGO3:*FHA-AGO3* line used, given that no *AGO3*-derived sRNAs were found in Col-0 *i.e.* non-transgenic plants. This lack of substantial overlap between AGO3 IP-isolated sRNAs and transcriptome may have several causes: (i) the mRNA sequencing may have mainly identified indirect targets of *AGO3* because the experiment was conducted on total siliques rather than isolated chalazal integument cells where *AGO3* is mostly, if not exclusively, expressed (Figure. 2), and/or (ii) sRNA-loaded AGO3 could act as translational repressors, in which case a lesser impact would be expected on target mRNA steady-state accumulation.

AGO3 localizes to the cytoplasm and co-sediments with polysomes

To strengthen our understanding of the molecular function of AGO3 in *Arabidopsis* cells, we investigated its intracellular localization. In *Arabidopsis*, AGO1 and AGO4 proteins are known to shuttle between the cytoplasm and the nucleus. However, their steady state localization seems to reflect their involvement in the TGS or PTGS pathways. Accordingly, AGO1 is mainly in the cytoplasm (Bologna *et al.*, 2018), whereas AGO4 mainly localizes to the nucleus (Ye *et al.*, 2012). We observed that the mCherry-AGO3 protein is cytoplasmic in both stamen filament and ovule integument cells (Figure 6). The cytoplasmic signal unlikely arises from a truncated mCherry-AGO3 protein because mainly a full-length fusion protein is detected in the transgenic lines used in this study (Figure S12).

To get deeper insights into the possible AGO3 mode(s) of action, we performed mass-spectrometry analysis of AGO3 co-immunoprecipitated proteins. Flag IPs were obtained on 1-5 DAP siliques from p*AGO3*:*FHA-AGO3*-expressing *ago3-3* plants, in two biological replicates. Flag IPs conducted in parallel in non-transgenic Col-0 siliques provided the negative controls. Only proteins displaying >2-fold enrichment in both biological replicates were selected, leading to a list of 79 AGO3 IP-enriched proteins (Table S2), including TUBULIN, which was previously found to interact with AGO3 (Chuong *et al.*, 2004). A GO-term enrichment analysis using agriGO (Du *et al.*, 2010) revealed a significant enrichment in NTP-dependent RNA helicases and core ribosomal constituents (Figure 7a). This finding prompted us to investigate whether AGO3 can indeed associate with ribosomes, either as

monosomes or polysomes, the latter reflecting active translation. Using conventional isolation procedures via differential centrifugation (Mustroph *et al.*, 2009) in 4-6 DAP siliques (Figure 7b) and in 1-5 DAP siliques (Figure S13), we found that AGO3 co-sediments with both monosomes and polysomes as was shown for several *Arabidopsis* AGOs including AGO1 and AGO5, which, like AGO3 binds both 24nt and 21nt sRNAs during silique development (Lanet *et al.*, 2009; Marchais *et al.*, 2019). These results suggest that AGO3 interacts with ongoing translation in siliques and could thus possibly regulate gene expression by PTGS *via* translational repression. Interestingly, previous work showed how an unconventional 24nt siRNA could guide translational repression of an HD-ZIP transcription factor mRNA in maize and of a GFP reporter in *Arabidopsis* (Klein-Cosson *et al.*, 2015), though the role of AGO3 in this process was not investigated in the study. Alternatively, AGO3 could be involved in both TGS and PTGS depending on the type or length of is sRNA cargoes. For example, it could direct TGS when loaded with intergenic small RNAs but PTGS when loaded with genic small RNAs. Its involvement in TGS could also be indirect via a sRNA binding competition that might exist between AGO3, AGO4 and AGO6 (all loading 24nt with 5'A). Further investigation will be necessary to untangle these possibilities.

EXPERIMENTAL PROCEDURES

Plant Materials and Growth Conditions

After three days at 4°C in the dark, seeds were germinated and grown on soil. Plants were grown under long days at 20-21°C (16h light/8h night). All plants were in Columbia (Col-0) accession. The mutants described in this work correspond to the following alleles: *ago1-27* (Morel *et al.*, 2002), *ago2-1* (Salk_037548), *ago3-2* (SALK_005335, (Takeda *et al.*, 2008)) *ago3-3* (GABI_743B03), *dcl1-11* (ZHANG *et al.*, 2008), *hen1-6* (SALK_090960, (Li *et al.*, 2005)), *hyl1-2* (Song *et al.*, 2007). The insertion lines were provided by The Nottingham Arabidopsis Stock Centre (NASC) (http://arabidopsis.info/).

Microscopy

Fluorescence images were acquired using laser scanning confocal microscopy (Zeiss LSM780) or

Leica epifluorescence microscope. Brightness and contrast were adjusted using ImageJ (http://rsbweb.nih.gov/ij/) and assembled using ImageJ or Adobe Photoshop.

Plasmid Construction and Transformation

All fragments were amplified by PCR using the Phusion High-Fidelity DNA Polymerase (Thermo). Primer sequences can be found in Supplementary Table S3. All plasmids were transformed into wild-type Columbia plants, *ago3-3, ago2-1,* and/or LIG1-GFP marker line (Andreuzza *et al.*, 2010). All constructs were generated using Multisite Gateway technology (Invitrogen). *A. thaliana* transformation was carried out by the floral dip method (Clough and Bent, 1998). At least ten transgenic lines were analyzed, which showed a consistent fluorescence using a Leica fluorescent microscope or consistent level of FlagHA by western blot. Three independent lines with single insertions, determined by segregation upon BASTA selection, were used for further detailed analysis.

RNA and qPCR analysis

Total RNA was extracted either with Qiagen RNeasy mini kit for silique samples or TRIzol reagent (Invitrogen) for other tissues. Total RNA was DNase treated (DNaseI, Thermo Scientific) and reverse transcribed into cDNA using the Maxima First-Strand cDNA Synthesis kit (Thermo Scientific). Results were normalized to *GAPC* levels for seedlings and to *GAPC* and/or *ACT11* for inflorescence and silique tissue. qPCR reactions were performed using KAPA fast Master Mix on a LightCycler480 II (Roche) or a Quantstudio5 (Thermo Scientific). Primers are listed in Table S3. The Relative Quantification value (RQ) represents the average RQ and the error bars represent standard error from at least two biological replicates. P values were calculated using a Student's t-test. Total RNA was depleted of ribosomic RNA and libraries prepared and subjected to paired-end sequencing using the corresponding Illumina protocols at the Functional Genomics Center Zurich (http://www.fgcz.ch/). For sRNA deep-sequencing analysis, sRNAs were eluted from the Flag beads using TRIzol and precipitated with glycogen and isopropanol overnight at -20°C. Total sRNAs and IP sRNAs were processed into sequencing libraries and sequenced by Fasteris (http://www.fasteris.com, Switzerland).

Protein and Immunoprecipitation analyses

Protein extraction and Western blot analysis were performed as previously described (Marí-Ordóñez *et al.*, 2013). Antibodies used in this paper are: Monoclonal ANTI-FLAG M2 Peroxidase HRP antibody (SIGMA A8592), Anti-HA-Peroxidase High Affinity 3F10 (ROCHE 12 013 819 001), anti-RFP (Chromotek 6G6), anti-Mouse HRP (abcam ab6789), S14 (Agrisera AS09 477), and Anti-AGO2 (Garcia *et al.*, 2012). For the native anti-AGO3, peptide antibodies were prepared in rabbits according to the DoubleX program of Eurogentec. Peptides used for AGO3 antibody production and immunization protocol were H-CRG FVQ DRD GGW VNP G-NH2 and H-CGH VRG RGT QLQ QPP P-NH2 both situated on the N-terminus of the AGO3 protein.

AGO3 protein immunoprecipitations were performed as previously described (Marí-Ordóñez *et al.*, 2013) with the following modifications: No preclearing was performed. Flag immunoprecipitation was performed using 30µl of EZview Red ANTI-FLAG M2 Affinity Gel from Sigma (SIGMA F2426) in 1.5ml lysate for 2-3h at 4C. Immunoprecipitation in non-transgenic plants or non-treated plants were used as a background control for all experiments. IP for the northern blot was conducted using anti-FLAG-conjugated agarose beads (Sigma) and the supernatant was pre-cleared for 15 minutes with 50µl of Protein A-agarose beads (Sigma).

For Mass spectrometry analysis, protein complexes were washed once with IP buffer and twice with 1X TBS buffer and subsequently eluted from the beads using competition with FLAG peptide according to the manufacturer's instructions (Sigma). The elution was precipitated, trypsin treated, and run using LC/ESI/MS/MS at the Functional Genomics Center Zurich. Mass spectrometry data analysis was performed using the Scaffold software (Proteome Software) with the following settings: Protein identification threshold of 5% FDR, minimum peptide 1, and peptide threshold 95%.

RNA blot analysis

RNA from input and IP samples, suspended in 50% formamide, was separated on a 17.5% polyacrylamide-urea gel, electrotransfered to a HyBond-NX membrane (GE Healthcare), and crosslinked with 1-ethyl-3-(3-dimethylaminopropyl) carbodiimide-mediated chemical crosslinking, as previously described (Pall and Hamilton, 2008). Radiolabeled probes were made by incubating gel-isolated PCR fragments with the Prime-A-Gene kit (Promega) in presence of [α-^{32}P]-dCTP (Hartmann Analytic). Multiple probes were tested on individual membranes by stripping with boiling

0.1% SDS and rehybridizing. Primers used to amplify the probes can be found in Supplementary Table S3.

Sucrose density gradient fractionation of polysomes

Sucrose gradients were conducted according to the protocol of Mustroph *et al* (Mustroph *et al.*, 2009). P170 correspond to the polysome resuspension after the sucrose cushion.

Bioinformatics

The Dot plot of Figure 1a was generated using CLC genomic workbench 8. Syntheny analysis were performed on the CoGe platform (Lyons and Freeling, 2008). Putative AGO protein sequences were downloaded from Phytozome (http://phytozome.jgi.doe.gov) (Goodstein *et al.*, 2012) with a double Pfam domain filter (PIWI, PF02171 and PAZ, PF02170). Prior to the analysis the sequences were cleaned using CD-HIT suite (http://weizhongli-lab.org/cd-hit/)(Huang *et al.*, 2010) using default parameters except for Sequence identity cut-off 1 and length of sequence to skip 500bp. Alignment and phylogenetic reconstructions were performed using the function "build" of ETE3 v3.0.0b32 (Huerta-Cepas *et al.*, 2016) as implemented on GenomeNet (https://www.genome.jp/tools/ete/) using default parameters. Alignment was performed with MAFFT v6.861b with the default options (Katoh and Standley, 2013). The tree was constructed using FastTree v2.1.8 with default parameters (Price *et al.*, 2009). Sequences used, SH-like local support at nodes as well as pmodeltest values can be found on the raw tree in Table S5. Phylogenic trees were visualized using CLC genomic workbench 8. Illustration for chromosomal loci positions, volcano plot and box plots were implemented with R and/or in-house scripts.

sRNA-seq analysis

For sRNA sequencing analysis, the trimmed sRNA reads were aligned against chloroplast, mitochondrial, rRNA, and tRNA sequences, and sequences of two chromosomal regions, which exhibit unusually high sRNA association (Chr2:1..10000 and Chr3:14194000..14204000) and which likely represent degradation products of spurious rDNA transcription. For alignment, bowtie (Langmead *et al.*, 2009) with the following parameters was used: -v 2 --best -m 1000. The unaligned reads were kept for further processing. Subsequently, all the reads shorter than 17 nt and longer than

30 nt were discarded using awk command (see Table S4a task A). We then aligned the filtered sRNA-seq reads against the TAIR10 *Arabidopsis thaliana* genome using bowtie with the following parameters: -v 2 --best -m 1000. TableS3b contains a summary of the read alignment scores. Using samtools sort and index (Li *et al.*, 2009), the resulting bam files were sorted and indexed. To determine the length distribution of entire libraries, bam files were converted to sam files (by samtools view) and the length distribution was extracted using a customized command line command based on the command line tool awk (see Table S4a task B).

Subsequently, the sum of sRNA-seq reads per 500 bp non-overlapping bin was assessed using HiCdat (Schmid *et al.*, 2015). For further analysis, genomic bins, which contained less than 5 reads in the total sRNA library were removed. The reads per bins values were normalized to the total read numbers across the libraries (using cpm() in the edgeR package (Robinson *et al.*, 2010)) To calculate the enrichment of AGO3 IPs, the number of reads per bin in the AGO3 IP was divided by the number of reads found in the total sRNA fraction. In parallel enrichment of the control FLAG IP over the total sRNA fraction was calculated. Later, significantly enriched bins had to fulfill following criteria: 10-fold enriched over the total sRNA fraction and less than 2-fold enrichment in the FLAG IP control fraction. For further analysis, sequences and coordinates of the significantly enriched bins were retrieved.

The first nucleotide of each alignment was obtained by customized awk script taking strand information of the alignment into account (for + alignments (see TableS3a task C); for – alignments see Table S4a task D). To resolve the first nucleotide identity by distinct sRNA sizes, above script was looped across sam files containing reads of a unique length only. To determine genomic features associated with the aligned sRNA reads, we extracted feature coordinates from the publicly available TAIR10 GFF3 file (TAIR10_GFF3_genes_transposons.gff, 49,811 kb, 2010-12-14). Using customized awk scripts, we added two features: promoters (500 bp up- and downstream of the start of the feature gene, respectively, depending on the genes orientation) (see Table S4a task E) and intergenic (all sequences that do not overlap the annotated GFF3 features and promoters), which were defined by using the bedtools complement tool (Quinlan and Hall, 2010) (complement of all features and entire chromosomes).

mRNA-seq analysis

For mRNA sequencing analysis, the filtered reads were aligned to the TAIR10 *Arabidopsis thaliana* genome using HISAT2 with default parameters (Kim *et al.*, 2015). After sorting and indexing using SAMTOOLS, the aligned RNA-seq reads were mapped to genomic features using the Rsubread (Liao *et al.*, 2013) package´s command RsubCounts() taking into account multi-mapping reads and strand specificity. The obtained gene read counts were subsequently analyzed for differential expression between the different genotypes (2 *ago3-3* homozygous, 2 *ago3-3* heterozygous, and 2 wild-type samples) using the edgeR (Robinson *et al.*, 2010) package. We only further analyzed genomic features, which exhibited at least 5 reads in at least 2 RNA-seq samples. The differential analysis was performed employing a linear model by using the estimateGLMCommonDisp() and estimateGLMTrendedDisp() functions. Differentially expressed features, which exhibited at least a 2-fold change and an FDR < 0.05 were scored as significantly differentially expressed.

For Figure 5e, microarray data from Belmonte *et al.* (Belmonte *et al.*, 2013) were extracted as pre-processed data from the Arabidopsis eFP Browser (Winter *et al.*, 2007). Expression means of the replicates were calculated for each transcript and represented as boxplots using R.

ACCESSION NUMBERS

Data sets of small RNAs and RNA deep-sequencing generated in this study are deposited in the National Center for Biotechnology Information Gene Expression Omnibus (http://www.ncbi.nlm.nih.gov/geo/) under accession number GSE124098.

ACKNOWLEDGEMENTS

We thank the Voinnet lab for thoughtful discussions, constructive ideas and critical reading of the manuscript. We additionally thank the following colleagues for their help: Andre Imboden and Jasmine Sekulovski for support concerning plant growth, Florian Brioudes and Christopher Brosnan for plasmids and advice during experiments. We thank Gina Cannarossi for her help and support for the phylogeny and syntheny analysis. This project was supported by a core grant from ETH-Z attributed to OV. PEJ (Project 329404), NP (Project 299789) and CC (Project 275589) were

supported by Marie Curie fellowships. PEJ and DMVB are supported by a grant from the SNF (163946).

AUTHOR CONTRIBUTIONS

PEJ conceived the project. OV contributed to the experimental design. PEJ, DMVB, NP, CC, CO and GS performed the research. SG and AM performed the bioinformatics analysis, together with PEJ. PEJ wrote the manuscript with the help of OV, NP and SG. PEJ and OV revised the manuscript.

CONFLICTS OF INTEREST

The authors have no conflicts of interest to declare.

SUPPORTING INFORMATION

Additional Supporting Information may be found in the online version of this article.

Figure S1. Additional syntheny analysis
Figure S2. Additional phylograms
Figure S3. AGOs alignments highlighting catalytic residues.
Figure S4. miR403 binding details
Figure S5. Additional qPCR supporting Figure 3 c-d
Figure S6. Western blot of FHA-AGO3 transgenic lines and AGO3 IPs in 1-5 DAP siliques
Figures S7. 5'nucleotide bias according to small RNA size
Figures S8. Representation of the sRNA sequencing reads for the loci tested by Northern blot in Figure 4f
Figure S9. AGO2 expression in *ago3-3* mutant
Figure S10. Absence of *ago3-3* reproductive phenotype.
Figure S11. Comparison between AGO3 enriched sRNA and *ago3-3* transcriptome
Figure S12. Western blot of mCherry-AGO3 transgenic lines
Figures S13. AGO3 co-sediments with polysomes in 1-5 DAP siliques

Table S1. GoTerm result of *ago3-3* differentially expressed genes

Table S2. Raw output from AGO3 IP Mass Spectometry

Table S3. Oligonucleotides used in this study.

Table S4. Bioinformatic analysis information.

Table S5. Additional phylogeny information.

REFERENCES

Allen, E., Xie, Z., Gustafson, A.M. and Carrington, J.C. (2005) microRNA-Directed Phasing during Trans-Acting siRNA Biogenesis in Plants. *Cell*, **121**, 207–221. Available at: http://linkinghub.elsevier.com/retrieve/pii/S0092867405003454.

Andreuzza, S., Li, J., Guitton, A.-E., Faure, J.-E., Casanova, S., Park, J.-S., Choi, Y., Chen, Z. and Berger, F. (2010) DNA LIGASE I exerts a maternal effect on seed development in Arabidopsis thaliana. *Development*, **137**, 73–81. Available at: http://www.ncbi.nlm.nih.gov/pubmed/20023162 [Accessed July 25, 2011].

Belmonte, M.F., Kirkbride, R.C., Stone, S.L., et al. (2013) Comprehensive developmental profiles of gene activity in regions and subregions of the Arabidopsis seed. *Proc. Natl. Acad. Sci. U. S. A.*, **110**, E435–E444. Available at: http://www.pubmedcentral.nih.gov/articlerender.fcgi?artid=3562769&tool=pmcentrez&rendertype=abstract [Accessed May 21, 2013].

Bologna, N.G., Iselin, R., Abriata, L.A., Sarazin, A., Pumplin, N., Jay, F., Grentzinger, T., Dal Peraro, M. and Voinnet, O. (2018) Nucleo-cytosolic Shuttling of ARGONAUTE1 Prompts a Revised Model of the Plant MicroRNA Pathway. *Mol. Cell*, **69**, 709-719.e5. Available at: https://doi.org/10.1016/j.molcel.2018.01.007.

Bologna, N.G. and Voinnet, O. (2014) The diversity, biogenesis, and activities of endogenous silencing small RNAs in Arabidopsis. *Annu. Rev. Plant Biol.*, **65**, 473–503. Available at: http://www.ncbi.nlm.nih.gov/pubmed/24579988.

Brosnan, C.A., Sarazin, A., Lim, P., Bologna, N.G., Hirsch-Hoffmann, M. and Voinnet, O. (2019) Genome-scale, single-cell-type resolution of micro RNA activities within a whole plant organ . *EMBO J.*, **38**, 1–19.

Buisine, N., Quesneville, H. and Colot, V. (2008) Improved detection and annotation of transposable elements in sequenced genomes using multiple reference sequence sets. *Genomics*, **91**, 467–475.

Carbonell, A., Fahlgren, N., Garcia-Ruiz, H., Gilbert, K.B., Montgomery, T. a, Nguyen, T., Cuperus, J.T. and Carrington, J.C. (2012) Functional analysis of three Arabidopsis ARGONAUTES using slicer-defective mutants. *Plant Cell*, **24**, 3613–29. Available at: http://www.pubmedcentral.nih.gov/articlerender.fcgi?artid=3480291&tool=pmcentrez&renderty

pe=abstract [Accessed October 9, 2014].

Chuong, S.D.X., Good, A.G., Taylor, G.J., Freeman, M.C., Moorhead, G.B.G. and Muench, D.G. (2004) Large-scale identification of tubulin-binding proteins provides insight on subcellular trafficking, metabolic channeling, and signaling in plant cells. *Mol. Cell. Proteomics*, **3**, 970–983.

Clough, S.J. and Bent, A.F. (1998) Floral dip: A simplified method for Agrobacterium-mediated transformation of *Arabidopsis thaliana*. *Plant J.*, **16**, 735–743.

Du, Z., Zhou, X., Ling, Y., Zhang, Z. and Su, Z. (2010) agriGO: A GO analysis toolkit for the agricultural community. *Nucleic Acids Res.*, **38**, 64–70.

Fahlgren, N., Montgomery, T.A., Howell, M.D., Allen, E., Dvorak, S.K., Alexander, A.L. and Carrington, J.C. (2006) Regulation of AUXIN RESPONSE FACTOR3 by TAS3 ta-siRNA Affects Developmental Timing and Patterning in Arabidopsis. *Curr. Biol.*, **16**, 939–944. Available at: http://www.ncbi.nlm.nih.gov/pubmed/16682356.

Garcia, D., Garcia, S., Pontier, D., Marchais, A., Renou, J.P., Lagrange, T. and Voinnet, O. (2012) Ago hook and RNA helicase motifs underpin dual roles for SDE3 in antiviral defense and silencing of nonconserved intergenic regions. *Mol. Cell*, **48**, 109–20. Available at: http://dx.doi.org/10.1016/j.molcel.2012.07.028 [Accessed September 10, 2013].

Goodstein, D.M., Shu, S., Howson, R., et al. (2012) Phytozome: a comparative platform for green plant genomics. *Nucleic Acids Res.*, **40**, D1178–D1186. Available at: http://nar.oxfordjournals.org/lookup/doi/10.1093/nar/gkr944.

Harvey, J.J.W., Lewsey, M.G., Patel, K., Westwood, J., Heimstädt, S., Carr, J.P. and Baulcombe, D.C. (2011) An antiviral defense role of AGO2 in plants. *PLoS One*, **6**, e14639. Available at: http://www.pubmedcentral.nih.gov/articlerender.fcgi?artid=3031535&tool=pmcentrez&rendertype=abstract [Accessed July 23, 2011].

Havecker, E.R., Wallbridge, L.M., Hardcastle, T.J., Bush, M.S., Kelly, K.A., Dunn, R.M., Schwach, F., Doonan, J.H. and Baulcombe, D.C. (2010) The Arabidopsis RNA-directed DNA methylation argonautes functionally diverge based on their expression and interaction with target loci. *Plant Cell*, **22**, 321–34. Available at:

http://www.plantcell.org/cgi/doi/10.1105/tpc.109.072199 [Accessed March 8, 2012].

Huang, Y., Niu, B., Gao, Y., Fu, L. and Li, W. (2010) CD-HIT Suite: A web server for clustering and comparing biological sequences. *Bioinformatics*, **26**, 680–682.

Huerta-Cepas, J., Serra, F. and Bork, P. (2016) ETE 3: Reconstruction, Analysis, and Visualization of Phylogenomic Data. *Mol. Biol. Evol.*, **33**, 1635–1638.

Iki, T., Tschopp, M.A. and Voinnet, O. (2017) Biochemical and genetic functional dissection of the P38 viral suppressor of RNA silencing. *Rna*, **23**, 639–654.

Jaubert, M., Bhattacharjee, S., Mello, A.F.S., Perry, K.L. and Moffett, P. (2011) ARGONAUTE2 mediates RNA-silencing antiviral defenses against Potato virus X in Arabidopsis. *Plant Physiol.*, **156**, 1556–1564. Available at: http://www.ncbi.nlm.nih.gov/pubmed/21576511 [Accessed July 20, 2011].

Katayama, H., Yamamoto, A., Mizushima, N., Yoshimori, T. and Miyawaki, A. (2008) GFP-like proteins stably accumulate in lysosomes. *Cell Struct. Funct.*, **33**, 1–12. Available at: http://www.ncbi.nlm.nih.gov/pubmed/18256512.

Katoh, K. and Standley, D.M. (2013) MAFFT multiple sequence alignment software version 7: Improvements in performance and usability. *Mol. Biol. Evol.*, **30**, 772–780.

Kim, D., Langmead, B. and Salzberg, S.L. (2015) HISAT: A fast spliced aligner with low memory requirements. *Nat. Methods*, **12**, 357–360.

Klein-Cosson, C., Chambrier, P., Rogowsky, P.M. and Vernoud, V. (2015) Regulation of a maize HD-ZIP IV transcription factor by a non-conventional RDR2-dependent small RNA. *Plant J.*, **81**, 747–758. Available at: http://doi.wiley.com/10.1111/tpj.12771.

Kremers, G.-J.G.-J., Gilbert, S.G., Cranfill, P.J., Davidson, M.W. and Piston, D.W. (2011) Fluorescent proteins at a glance. *J. Cell Sci.*, **124**, 2676–2676. Available at: http://jcs.biologists.org/cgi/doi/10.1242/jcs.095059.

Lanet, E., Delannoy, E., Sormani, R., Floris, M., Brodersen, P., Crété, P., Voinnet, O. and Robaglia, C. (2009) Biochemical Evidence for Translational Repression by Arabidopsis MicroRNAs. *Plant Cell*, **21**, 1762–8. Available at: http://www.ncbi.nlm.nih.gov/pubmed/19531599.

Langmead, B., Trapnell, C., Pop, M. and Salzberg, S.L. (2009) Ultrafast and memory-efficient

alignment of short DNA sequences to the human genome. *Genome Biol.*, **10**.

Law, J.A. and Jacobsen, S.E. (2010) Establishing , maintaining and modifying DNA methylation patterns in plants and animals. *Nat. Rev. Genet.*, **11**, 204–220. Available at: http://www.nature.com/doifinder/10.1038/nrg2719.

Li, H., Handsaker, B., Wysoker, A., Fennell, T., Ruan, J., Homer, N., Marth, G., Abecasis, G. and Durbin, R. (2009) The Sequence Alignment/Map format and SAMtools. *Bioinformatics*, **25**, 2078–2079.

Li, J., Yang, Z., Yu, B., Liu, J. and Chen, X. (2005) Methylation Protects miRNAs and siRNAs from a 3′-End Uridylation Activity in Arabidopsis. *Curr. Biol.*, **15**, 1501–1507. Available at: http://linkinghub.elsevier.com/retrieve/pii/S0960982205007736.

Liao, Y., Smyth, G.K. and Shi, W. (2013) The Subread aligner: Fast, accurate and scalable read mapping by seed-and-vote. *Nucleic Acids Res.*, **41**, e108–e108.

Liu, Q., Yao, X., Pi, L., Wang, H., Cui, X. and Huang, H. (2009) The ARGONAUTE10 gene modulates shoot apical meristem maintenance and establishment of leaf polarity by repressing miR165/166 in Arabidopsis. *Plant J.*, **58**, 27–40.

Lyons, E. and Freeling, M. (2008) How to usefully compare homologous plant genes and chromosomes as DNA sequences. *Plant J.*, **53**, 661–673.

Mallory, A. and Vaucheret, H. (2010) Form, function, and regulation of ARGONAUTE proteins. *Plant Cell*, **22**, 3879–89. Available at: http://www.pubmedcentral.nih.gov/articlerender.fcgi?artid=3027166&tool=pmcentrez&rendertype=abstract [Accessed May 22, 2013].

Marchais, A., Chevalier, C. and Voinnet, O. (2019) Extensive profiling in Arabidopsis reveals abundant polysome-associated 24-nt small RNAs including AGO5-dependent pseudogene-derived siRNAs . *Rna*, **25**, 1098–1117.

Marí-Ordóñez, A., Marchais, A., Etcheverry, M., Martin, A., Colot, V. and Voinnet, O. (2013) Reconstructing de novo silencing of an active plant retrotransposon. *Nat. Genet.*, **45**, 1029–39. Available at: http://www.ncbi.nlm.nih.gov/pubmed/23852169.

Maunoury, N. and Vaucheret, H. (2011) AGO1 and AGO2 act redundantly in miR408-mediated Plantacyanin regulation. *PLoS One*, **6**.

Mi, S., Cai, T., Hu, Y., et al. (2008) Sorting of small RNAs into Arabidopsis argonaute complexes is directed by the 5' terminal nucleotide. *Cell*, **133**, 116–27. Available at: http://dx.doi.org/10.1016/j.cell.2008.02.034 [Accessed June 11, 2011].

Montgomery, T.A., Howell, M.D., Cuperus, J.T., et al. (2008) Specificity of ARGONAUTE7-miR390 Interaction and Dual Functionality in TAS3 Trans-Acting siRNA Formation. *Cell*, **133**, 128–141.

Morel, J., Godon, C., Mourrain, P., Feuerbach, F. and Proux, F. (2002) Fertile Hypomorphic ARGONAUTE (ago1) Mutants Impaired in Post-Transcriptional Gene Silencing and Virus Resistance. *Plant Cell*, **14**, 629–639.

Mustroph, A., Juntawong, P. and Bailey-serres, J. (2009) Isolation of Plant Polysomal mRNA by Differential Centrifugation and Ribosome Immunopurification Methods. *Methods Mol. Biol.*, **553**, 109–126. Available at: http://link.springer.com/10.1007/978-1-60327-563-7.

Nikolov, L.A., Shushkov, P., Nevado, B., Gan, X., Al-Shehbaz, I.A., Filatov, D., Bailey, C.D. and Tsiantis, M. (2019) Resolving the backbone of the Brassicaceae phylogeny for investigating trait diversity. *New Phytol.*, **222**, 1638–1651.

Olmedo-Monfil, V., Durán-Figueroa, N., Arteaga-Vázquez, M., Demesa-Arévalo, E., Autran, D., Grimanelli, D., Slotkin, R.K., Martienssen, R.A. and Vielle-Calzada, J.-P. (2010) Control of female gamete formation by a small RNA pathway in Arabidopsis. *Nature*, **464**, 628–632. Available at: http://www.nature.com/doifinder/10.1038/nature08828.

Pall, G.S. and Hamilton, A.J. (2008) Improved northern blot method for enhanced detection of small RNA. *Nat. Protoc.*, **3**, 1077–1084.

Poulsen, C., Vaucheret, H. and Brodersen, P. (2013) Lessons on RNA Silencing Mechanisms in Plants from Eukaryotic Argonaute Structures. *Plant Cell*, **25**, 22–37. Available at: http://www.ncbi.nlm.nih.gov/pubmed/23303917 [Accessed March 1, 2013].

Price, M.N., Dehal, P.S. and Arkin, A.P. (2009) Fasttree: Computing large minimum evolution trees with profiles instead of a distance matrix. *Mol. Biol. Evol.*, **26**, 1641–1650.

Pumplin, N. and Voinnet, O. (2013) RNA silencing suppression by plant pathogens: defence, counter-defence and counter-counter-defence. *Nat. Rev. Microbiol.*, **11**, 745–60. Available at: http://www.nature.com/doifinder/10.1038/nrmicro3120 [Accessed November 8, 2013].

Quinlan, A.R. and Hall, I.M. (2010) BEDTools: A flexible suite of utilities for comparing genomic features. *Bioinformatics*, **26**, 841–842.

Robinson, M.D., McCarthy, D.J. and Smyth, G.K. (2010) edgeR: a Bioconductor package for differential expression analysis of digital gene expression data. *Bioinformatics*, **26**, 139–140. Available at: http://bioinformatics.oxfordjournals.org/cgi/doi/10.1093/bioinformatics/btp616.

Schmid, M.W., Grob, S. and Grossniklaus, U. (2015) HiCdat: A fast and easy-to-use Hi-C data analysis tool. *BMC Bioinformatics*, **16**, 1–6. Available at: http://dx.doi.org/10.1186/s12859-015-0678-x.

Song, L., Han, M.H., Lesicka, J. and Fedoroff, N. (2007) Arabidopsis primary microRNA processing proteins HYL1 and DCL1 define a nuclear body distinct from the Cajal body. *Proc. Natl. Acad. Sci. U. S. A.*, **104**, 5437–5442.

Takeda, A., Iwasaki, S., Watanabe, T., Utsumi, M. and Watanabe, Y. (2008) The mechanism selecting the guide strand from small RNA duplexes is different among Argonaute proteins. *Plant Cell Physiol.*, **49**, 493–500. Available at: http://www.ncbi.nlm.nih.gov/pubmed/18344228 [Accessed June 11, 2011].

Tucker, M.R., Okada, T., Hu, Y., Scholefield, A., Taylor, J.M. and Koltunow, A.M.G. (2012) Somatic small RNA pathways promote the mitotic events of megagametogenesis during female reproductive development in Arabidopsis. *Development*, **139**, 1399–1404. Available at: http://dev.biologists.org/cgi/doi/10.1242/dev.075390 [Accessed March 9, 2012].

Wei, W., Ba, Z., Gao, M., et al. (2012) A Role for Small RNAs in DNA Double-Strand Break Repair. *Cell*, **2**, 1–12. Available at: http://linkinghub.elsevier.com/retrieve/pii/S0092867412002954 [Accessed March 22, 2012].

Winter, D., Vinegar, B., Nahal, H., Ammar, R., Wilson, G. V. and Provart, N.J. (2007) An "electronic fluorescent pictograph" Browser for exploring and analyzing large-scale biological data sets. *PLoS One*, **2**, 1–12.

Ye, R., Wang, W., Iki, T., Liu, C., Wu, Y., Ishikawa, M., Zhou, X. and Qi, Y. (2012) Cytoplasmic Assembly and Selective Nuclear Import of Arabidopsis ARGONAUTE4/siRNA Complexes. *Mol. Cell*, **46**, 859–870. Available at: http://dx.doi.org/10.1016/j.molcel.2012.04.013.

ZHANG, J.-F., Yuan, L.-J., SHAO, Y., DU, W., Yan, D.-W. and LU, Y.-T. (2008) The

disturbance of small RNA pathways enhanced abscisic acid response and multiple stress responses in Arabidopsis. *Plant. Cell Environ.*, **31**, 562–574. Available at: http://doi.wiley.com/10.1111/j.1365-3040.2008.01786.x.

Zhang, X., Zhao, H., Gao, S., Wang, W.C., Katiyar-Agarwal, S., Huang, H. Da, Raikhel, N. and Jin, H. (2011) Arabidopsis Argonaute 2 Regulates Innate Immunity via miRNA393*-Mediated Silencing of a Golgi-Localized SNARE Gene, MEMB12. *Mol. Cell*, **42**, 356–366. Available at: http://dx.doi.org/10.1016/j.molcel.2011.04.010.

Zhang, Z., Liu, X., Guo, X., Wang, X.-J. and Zhang, X. (2016) Arabidopsis AGO3 predominantly recruits 24-nt small RNAs to regulate epigenetic silencing. *Nat. Plants*, 16049. Available at: http://www.nature.com/articles/nplants201649.

Zheng, X., Zhu, J., Kapoor, A. and Zhu, J.-K. (2007) Role of Arabidopsis AGO6 in siRNA accumulation, DNA methylation and transcriptional gene silencing. *EMBO J.*, **26**, 1691–1701.

Zhong, X., Du, J., Hale, C.J., et al. (2014) Molecular mechanism of action of plant DRM de novo DNA methyltransferases. *Cell*, **157**, 1050–1060. Available at: http://dx.doi.org/10.1016/j.cell.2014.03.056 [Accessed July 29, 2014].

Zhu, H., Hu, F., Wang, R., Zhou, X., Sze, S.-H., Liou, L.W., Barefoot, A., Dickman, M. and Zhang, X. (2011) Arabidopsis Argonaute10 specifically sequesters miR166/165 to regulate shoot apical meristem development. *Cell*, **145**, 242–56. Available at: http://www.ncbi.nlm.nih.gov/pubmed/21496644 [Accessed July 17, 2011].

Zilberman, D., Cao, X. and Jacobsen, S.E. (2003) ARGONAUTE4 control of locus-specific siRNA accumulation and DNA and histone methylation. *Science*, **299**, 716–9. Available at: http://www.ncbi.nlm.nih.gov/pubmed/12522258.

FIGURE LEGENDS

Figure 1. *AGO3* and *AGO2* arose from a recent duplication of the coding region.
(a) Dot plot visualization of the alignment of the *AGO2/AGO3* locus to itself showing that the duplication happens at the Glycine rich repeats and comprises the coding sequence but not the promoter. (b) Snap shot of GEvo Syntheny Browser (CoGe) showing synteny of the *A.thaliana AGO2/AGO3* locus with *C.rubella* but not *C. hirsuta.* (c) Circular phylogram showing that the duplication exists in *Arabidopsis* and in *Capsella* but not in *E. salsugineum*. The *AGO1/5/10* and *AGO4/6/8/9* branches are collapsed.

Figure 2. AGO3 and AGO2 display cell specific expression in reproductive tissues
(a-f) Confocal images from transgenic plants expressing a *pAGO3:mCherry-AGO3* (a-d) and *pAGO2:mCherry-AGO2* (e-f). mCherry-AGO3 is expressed in the chalazal integument in ovules (a) and seeds (b); at the end of stamen filaments (c) and at the base of the floral meristem (d). mCherry-AGO2 is expressed in the egg cell (e) and sperm cells(f). Scale bars are shown as a white rectangle. czi-chalazal integument, s-sperm cells, ec-egg cell, cc-central cell; syn-synergids; asterisks correspond to autofluorescence; DIC-Differential-Interference-Contrast.

Figure 3. *AGO2* and *AGO3* regulation by mir403 affect expression level but not pattern.
(a) Epifluorescence images showing *pAGO2:H2B-mCherry* expression in the egg cell and sperm cells. (b) Confocal images showing *pAGO3:H2B-mCherry* expression in the chalazal integument of the ovule. *pAGO3:H2B-mCherry* is also expressed at the base of flower primordia and end of stamen filament. Epifluorescence images showing *pAGO3:H2B-mCherry* expression in seed. (c) qPCR showing upregulation of *AGO3* in *ago1-27*, *dcl1-11, hyl1-2* and *hen1-6* mutant in inflorescences. (d) qPCR showing upregulation of *AGO2* in *ago1-27*, *dcl1-11, hyl1-2* and *hen1-6* mutant inflorescences. (c-d) The histogram represents the mean value of three biological replicates which are represented as dots. *ACT11 was* used as normalizer for qPCR. *p* indicates the *p* value obtained after a Student's t-test compared to Col-0.

Figure 4. Characterization of AGO3-bound small RNA

(a) Northern blot showing that FHA-AGO3 can bind both 21nt and 24 nt sRNAs in transient expression in *N. benthamiana*. (b-e), AGO3-bound sRNAs were obtained by deep sequencing of a Flag IP on 1-5 DAP silique samples of *ago3-3 pAGO3:FHA-AGO3* transgenic plants. (b) AGO3 binds preferentially sRNAs with 5'A. (c) AGO3 binds 21- but preferentially 24-nucleotide sRNAs. (d) Chromosomic distribution of AGO3 bound sRNA. (e) Functional annotation of AGO3 bound sRNA. (f) Northern blot analysis of sRNAs after Flag IP in 4-6 DAP siliques of Col-0, *ago3-3 pAGO3:FHA-AGO3* and *ago2-1 pAGO2:FHA-AGO2* compared with input control.

Figure 5. Transcriptome analysis of *ago3-3* mutant

(a) q-PCR analysis of *AGO3* expression in different tissues. Error bars represents standard error of two or three biological replicates. *p* indicates the *p* value obtained from a Student's t-test. (b) Western blot analysis of AGO3 protein accumulation in different tissues and indicated genotype. (c) volcano plot showing the 87 mis-expressed genes in *ago3-3* compared to Col-0 1-5DAP siliques. (d) genomic location of *ago3-3* mis-expressed genes (down regulated genes are represented by red triangle and up regulated genes are represented by blue triangle). (e-f) Expression time course of up-regulated (e) and down (f) regulated genes in the chalazal seed coat at different stages of seed development. (g) Pictures and quantification of seed abortion at the green seed stage of Col-0, *ago3-3* and *ago3-1*. Lv, leaves; cLv, cauline leaves; Inflo, Inflorescence; DAP, day after pollination

Figure 6. AGO3 localizes to the cytoplasm

Confocal imaging showing *pAGO3:mCherry-AGO3* localisation in the cytoplasm of cells in the stamen filament as well as ovule integuments. *LIG1-GFP* is used as a DNA marker. n, nucleus; c, cytoplasm.

Figure 7. AGO3 co-sediments with the translation machinery.

(a) Go-term enrichment of putative AGO3 interactors identified by mass spectrometry analysis of *ago3-3 pAGO3:FHA-AGO3* Flag IP in 1-5 DAP siliques. (b) Western blot analysis of polysome fractionation on 4-6 DAP siliques showing the co-sedimentation of AGO3 with monosomes and

polysomes. P170 represents the fraction loaded onto the sucrose gradient (ie *the polysome resuspension after the sucrose cushion)*. The ribosomic protein S14 is used as a control to follow the sedimentation of ribosomes within the sucrose gradient.

Figure S1. Additional syntheny analysis

Snap shot of GEvo Synteny Browser (CoGe) showing synteny of the *A.thaliana AGO2/AGO3* locus with *C. rubella* and *B.stricta* but not *C. hirsuta*, *T. halophila* and *A. Alpina*. The duplication seems absent in *E. Cheianthoides* (caution: in *E. Cheianthoides* the *AGO2/AGO3* locus is situated in a non-annotated/non-assembled scaffold). Tree illustration on the left correspond to *Brassicaceae* lineages from Nikolov *et al* 2019.

Figure S2. Additional phylograms.

(a) Uncollapsed Circular phylogram from Figure 1. Sequences used to build this tree were all obtained from http://phytozome.jgi.doe.gov/pz/portal.html and only putative proteins containing both PAZ and PIWI pfam domains were used. Classical Arabidopsis AGOs clades are represented: AGO2/3/7 in green, AGO4/6/8/9 in purple and AGO1/5/10 in blue. Original protein sequence names from Phytozome are shown. (b) Radial representation of the tree represented in Figure S2a emphasizing the different clades of plant Argonautes.

Figure S3. AGOs alignments highlighting catalytic residues.

(a) Alignment of *Arabidopsis* Argonaute PIWI active residues (Red: catalytic residues, green: 5' binding pocket residues). Highlighted residues show the unique DNDD motif of AGO3 and AGO2 as annotated on NCBI CDD cd02826 (http://www.ncbi.nlm.nih.gov/Structure/cdd/cddsrv.cgi?hslf=1&uid=cd02826).

(b) Alignment of Argonaute PIWI active residues of the AGO2/AGO3 clade (Corresponding to the DDD AGOs clade in Figure 1 and Figure S2) highlighting their conserved DDD motif.

Figure S4. miR403 binding details

Localisation and sequence of the putative binding site of miR403 within *AGO2* (a) and *AGO3* (b) 3'UTR.

Figure S5. Additional replicate experiment from Figure 3 c-d

(a) qPCR showing upregulation of *AGO3* in *ago1-27*, *dcl1-11* and *hen1-6* mutant in inflorescences. (b) qPCR showing upregulation of *AGO2* in *ago1-27*, *dcl1-11* and *hen1-6* mutant inflorescences. (a-b) Error bar represents standard deviation of two or three biological replicates. ACT11/GAPC were used as normalizer for qPCR. p indicates the p value obtained after a Student's t-test compared to Col-0.

Figure S6. FHA-AGO3 Western blot

(a) Western blot detection of the full-length FHA-AGO3 tagged protein in pAGO3:FHA-AGO3 and p35S:FHA-AGO3 transgenic lines. Strong accumulation of a cleaved FHA-AGO3 fragment can be in overexpressing lines. Amount of the full length FHA-AGO3 is similar to the one observed in Col-0 in Figure5b. L-Leaves, B-Buds and S-Siliques. (b) IP done in siliques from 1 to 5 DAP of *ago3-3 pAGO3:FHA-AGO3* transgenic plants. (a-b) Anti-HA antibody (a) and Anti-Flag antibody (b) were used to detect tagged AGO3 and Coomassie staining is used as loading control.

Figure S7. 5'nucleotide bias according to small RNA size

5' nucleotide bias according to the small RNA size in the sequencing libraries as well as IP enriched fractions.

Figure S8. Representation of the sRNA sequencing reads for six "AGO3-enriched" loci. (a) the loci tested by northern blot in Figure 4f. (b) three enriched loci showing specific microRNA-like enrichment peak.

Figure S9. AGO2 expression in *ago3-3* mutant.

Western blot analysis of AGO2 protein accumulation in different tissues and indicated genotype.

Figure S10. Absence of *ago3-3* reproductive phenotype.

(a-b) No significative change of seed size was observed between Col-0 and *ago3-3* mutant either in self-fertilization (a) or in reciprocal crosses condition (b). Seed size was quantified using Image J. Area is in μm^2. (c) No significative changes in seed permeability was observed in between Col-0 and *ago3-1* mutant using tetrazolium assay (Debeaujon et al, 2000). (d) No embryo developmental timing defect was observed at 4 Days after pollination in between Col-0 and *ago3-3* or *ago3-1* mutant. Seeds were cleared in Chloral hydrate and observed under Differential-Interference-Contrast.

Figure S11. Comparison between AGO3 enriched sRNA and *ago3-3* transcriptome

(a) Venn diagram showing a lack of overlap between AGO3 enriched small RNA and the differentially expressed genes (DEG) in-between Col-0 and *ago3-3* mutant either using overlap with the coding sequence (CDS) or 1kb promoter sequences. (b) sRNA coverage at the *AGO3* locus (*At1g31290*).

Figure S12. mCherry-AGO3 Western blot

Western blot detection of the full-length mCherry-AGO3 tagged protein in *pAGO3:mCherry-AGO3* transgenic lines in 1-5 DAP siliques. A cleaved mCherry-AGO3 fragment is barely detectable compared to the full length mCherry-AGO3 protein. Anti-mCherry antibody was used to detect tagged AGO3 and Coomassie staining is used as loading control.

Figure S13. AGO3 co-sediments with polysomes at 1-5 DAP

(a) Polysome fractionation showing the co-sedimentation of AGO3 with monosomes and polysomes in 1-5 DAP siliques. P170 represents the fraction loaded onto the sucrose gradient (ie *the polysome resuspension after the sucrose cushion)*. The ribosomic protein S14 is used as a control to follow the sedimentation of ribosomes within the sucrose gradient.

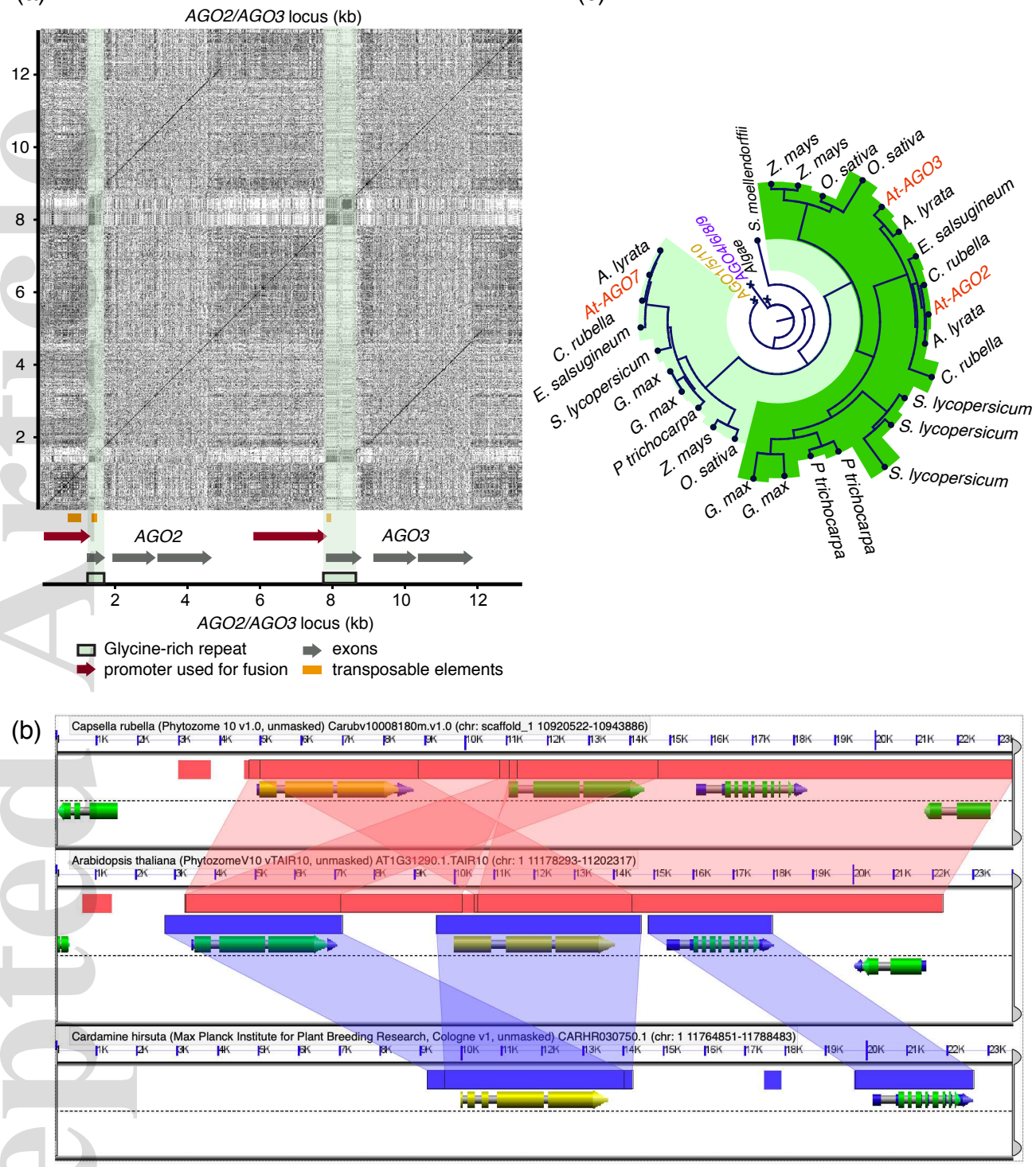

Figure 1. AGO3 and AGO2 arose from a recent duplication of the coding region. (a) Dot plot visualization of the alignment of the AGO2/AGO3 locus to itself showing that the duplication happens at the Glycine rich repeats and comprises the coding sequence but not the promoter. (b) Snap shot of GEvo Syntheny Browser (CoGe) showing synteny of the A.thaliana AGO2/AGO3 locus with C.rubella but not C. hirsuta. (c) Circular phylogram showing that the duplication exists in Arabidopsis and in Capsella but not in E. salsugineum. The AGO1/5/10 and AGO4/6/8/9 branches are collapsed.

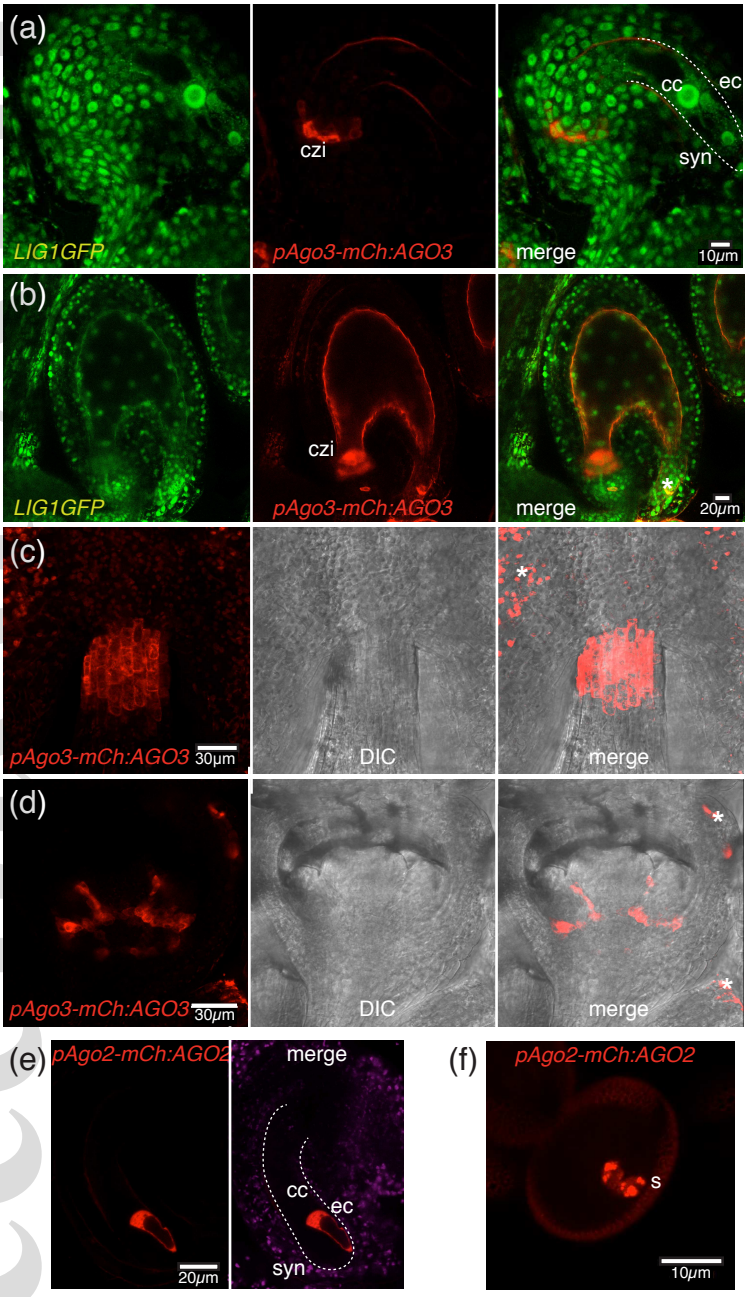

Figure 2. AGO3 and AGO2 display cell specific expression in reproductive tissues

(a-f) Confocal images from transgenic plants expressing a pAGO3:mCherry-AGO3 (a-d) and pAGO2:mCherry-AGO2 (e-f). mCherry-AGO3 is expressed in the chalazal integument in ovules (a) and seeds (b); at the end of stamen filaments (c) and at the base of the floral meristem (d). mCherry-AGO2 is expressed in the egg cell (e) and sperm cells(f). Scale bars are shown as a white rectangle. czi-chalazal integument, s-sperm cells, ec-egg cell, cc-central cell; syn-synergids; asterisks correspond to autofluorescence; DIC-Differential-Interference-Contrast.

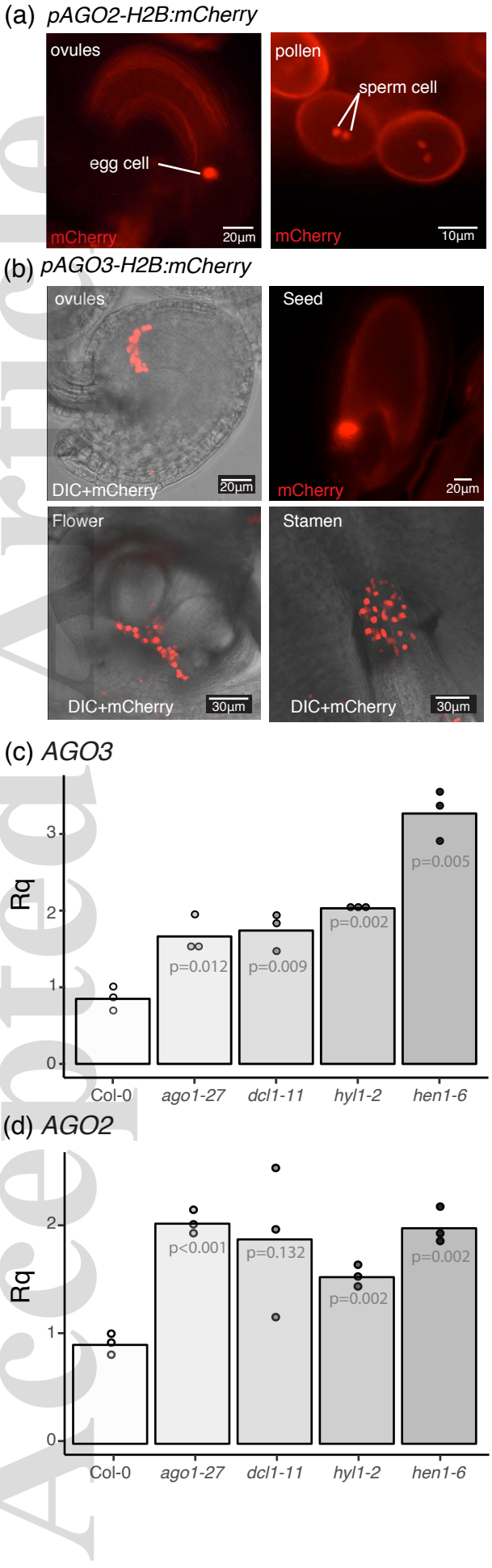

Figure 3. AGO2 and AGO3 regulation by mir403 affect expression level but not pattern.
(a) Epifluorescence images showing pAGO2:H2B-mCherry expression in the egg cell and sperm cells. (b) Confocal images showing pAGO3:H2B-mCherry expression in the chalazal integument of the ovule. pAGO3:H2B-mCherry is also expressed at the base of flower primordia and end of stamen filament. Epifluorescence images showing pAGO3:H2B-mCherry expression in seed. (c) qPCR showing upregulation of AGO3 in ago1-27, dcl1-11, hyl1-2 and hen1-6 mutant in inflorescences. (d) qPCR showing upregulation of AGO2 in ago1-27, dcl1-11, hyl1-2 and hen1-6 mutant inflorescences. (c-d) The histogram represent the mean value of three biological replicates which are represented as dots. ACT11 was used as normalizer for qPCR. p indicates the p value obtained after a Student's t-test compared to Col-0.

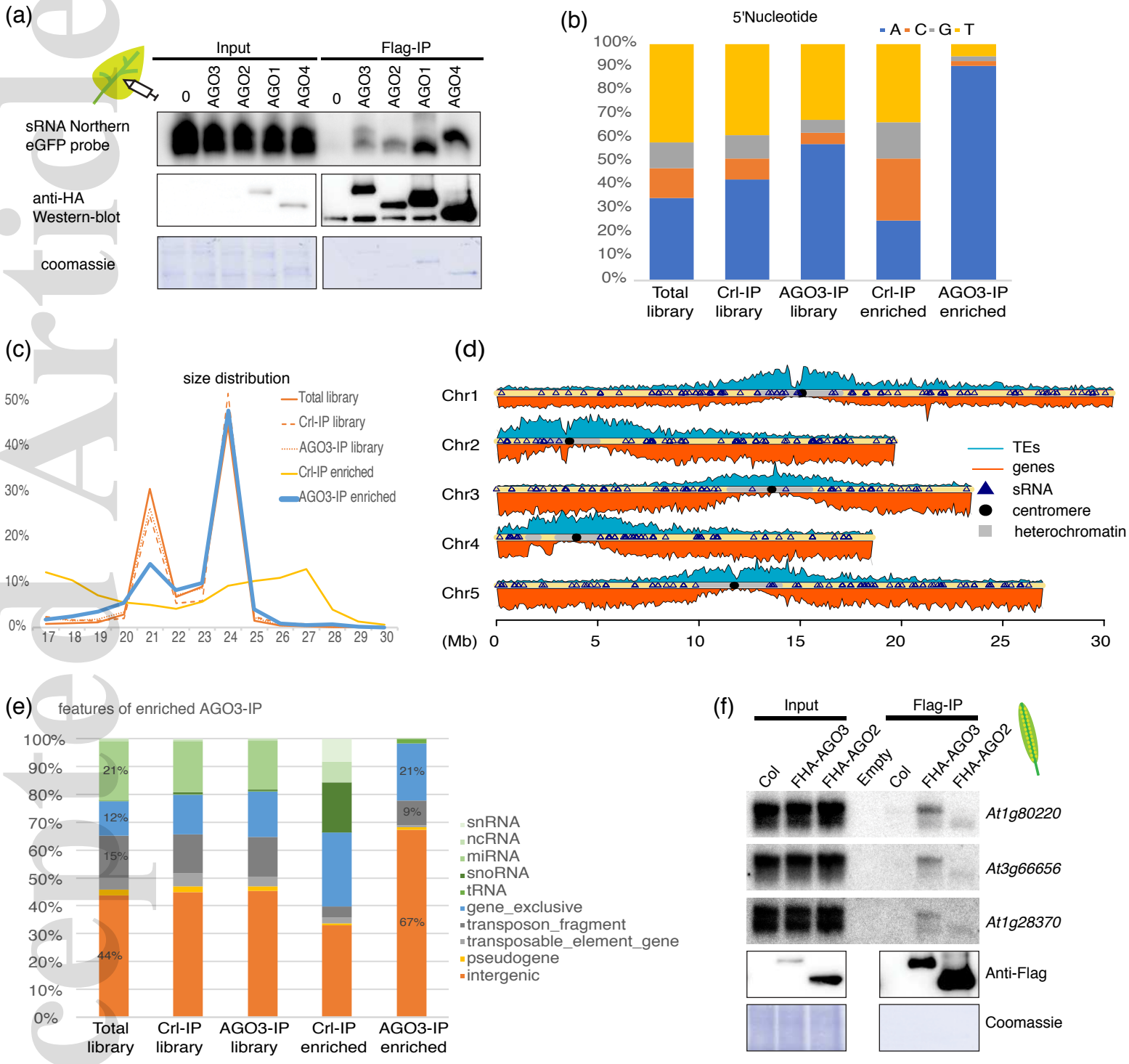

Figure 4. Characterization of AGO3-bound small RNA

(a) Northern blot showing that FHA-AGO3 can bind both 21nt and 24 nt sRNAs in transient expression in N. benthamiana. (b-e), AGO3-bound sRNAs were obtained by deep sequencing of a Flag IP on 1-5 DAP silique samples of ago3-3 pAGO3:FHA-AGO3 transgenic plants. (b) AGO3 binds preferentially sRNAs with 5'A. (c) AGO3 binds 21- but preferentially 24-nucleotide sRNAs. (d) Chromosomic distribution of AGO3 bound sRNA. (e) Functional annotation of AGO3 bound sRNA. (f) Northern blot analysis of sRNAs after Flag IP in 4-6 DAP siliques of Col-0, ago3-3 pAGO3:FHA-AGO3 and ago2-1 pAGO2:FHA-AGO2 compared with input control.

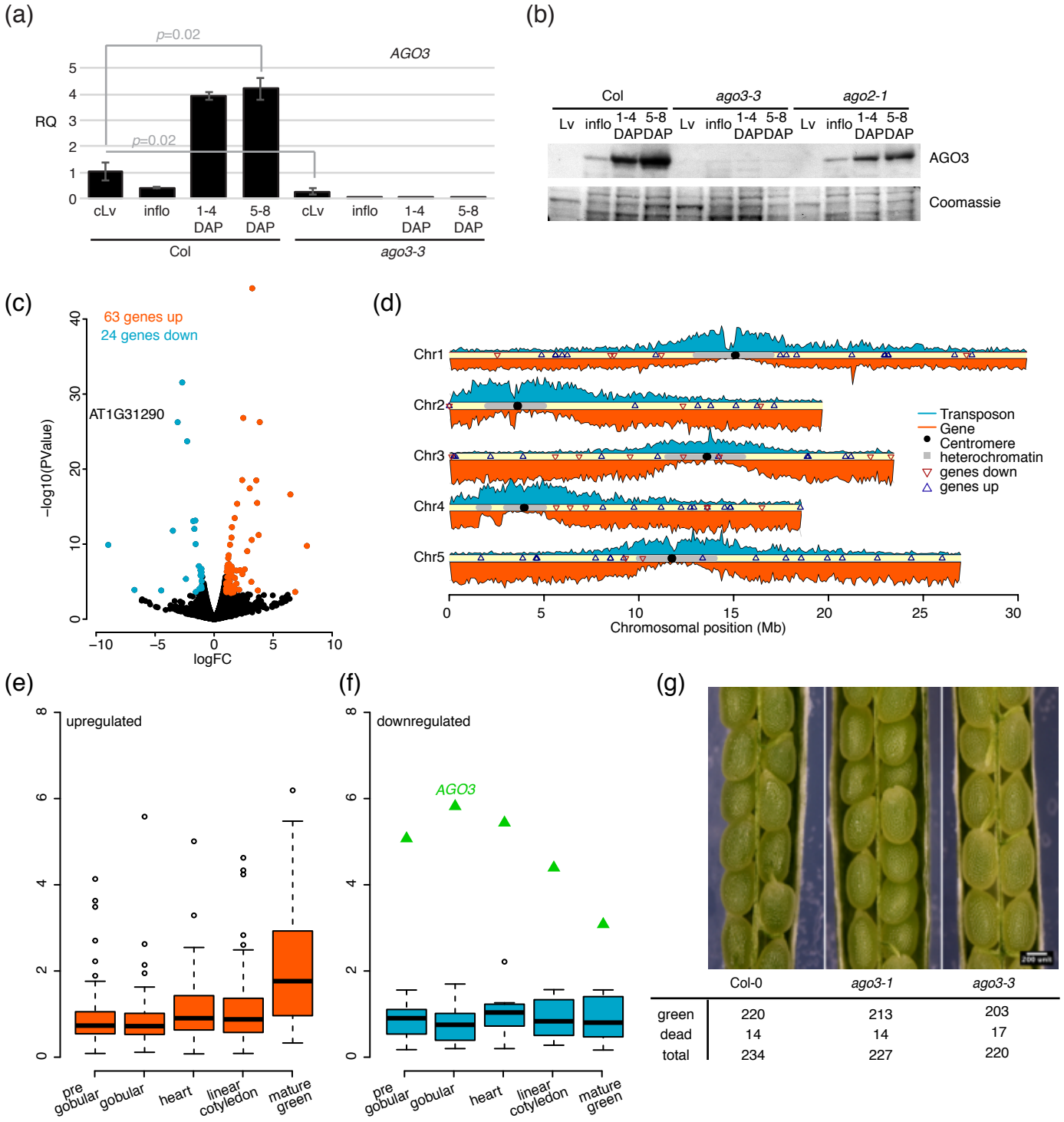

Figure 5. Transcriptome analysis of ago3-3 mutant

(a) q-PCR analysis of AGO3 expression in different tissues. Error bars represents standard error of two or three biological replicates. p indicates the p value obtained from a Student's t-test. (b) Western blot analysis of AGO3 protein accumulation in different tissues and indicated genotype. (c) volcano plot showing the 87 mis-expressed genes in ago3-3 compared to Col-0 1-5DAP siliques. (d) genomic location of ago3-3 mis-expressed genes (down regulated genes are represented by red triangle and up regulated genes are represented by blue triangle). (e-f) Expression time course of up-regulated (e) and down (f) regulated genes in the chalazal seed coat at different stages of seed development. (g) Pictures and quantification of seed abortion at the green seed stage of Col-0, ago3-3 and ago3-1. Lv, leaves; cLv, cauline leaves; Inflo, Inflorescence; DAP, day after pollination

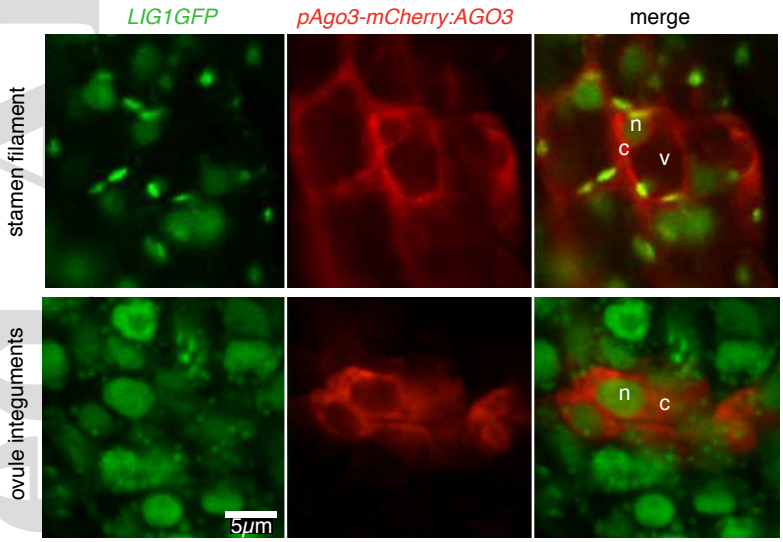

Figure 6. AGO3 localize to the cytoplasm
Confocal imaging showing pAGO3:mCherry-AGO3 localisation in the cytoplasm of cells in the stamen filament as well as ovule integuments. LIG1-GFP is used as a DNA marker. n, nucleus; c, cytoplasm.

(a)

GO-term Silique IP Mass-spec	p-value
structural molecule activity	3.60E-14
structural constituent of ribosome	3.80E-11
ATP-dependent helicase activity	8.50E-06
purine NTP-dependent helicase activity	8.50E-06
helicase activity	4.40E-05

(b)

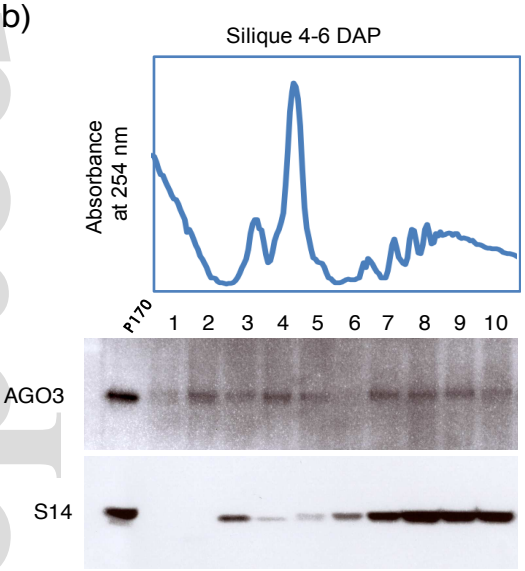

Figure 7. AGO3 co-sediments with the translation machinery.
(a) Go-term enrichment of putative AGO3 interactors identified by mass spectrometry analysis of ago3-3 pAGO3:FHA-AGO3 Flag IP in 1-5 DAP siliques. (b) Western blot analysis of polysome fractionation on 4-6 DAP siliques showing the co-sedimentation of AGO3 with monosomes and polysomes.